Discover Applied Sciences

Research

Failure pressure prediction of high-strength steel pipe bend considering pipe and corrosion geometry

Suria Devi Vijaya Kumar[1] · Saravanan Karuppanan[1] · Veeradasan Perumal[1] · Mark Ovinis[2]

Received: 19 December 2023 / Accepted: 12 March 2024
Published online: 25 March 2024

Abstract
This study examines the influence of pipe bend geometry and corrosion geometry on the failure pressure of high-strength steel pipe bends subjected to internal pressure and axial compressive stress. Finite element analysis determines the impact of bend angle, bending radius, defect depth, defect length, defect spacing, and axial compressive stress on failure pressures. The findings reveal that increasing the bend angle reduces failure pressures significantly, with corrosion defects exacerbating this effect. Increased bending radius increases normalized failure pressure from 0.88 to 0.91 for intrados defects and decreases it from 0.98 to 0.93 for extrados defects. Additionally, single defects cause a slight 2.5–3.0% reduction in normalized failure pressure, while longitudinally and circumferentially aligned defects result in a 13–15% decrease in normalized failure pressure. Defect depth and length also significantly influence the failure pressure, particularly for deeper and longer defects (up to 48.2%). Furthermore, an empirical equation for predicting failure pressures in corroded pipe bends with high accuracy ($R^2 = 0.99$) is developed based on Artificial Neural Network. This enhances pipeline integrity assessment and design practices.

Article Highlights

- Corrosion and pipe geometry significantly affect pipe failure pressure, with bends experiencing greater reduction in pressure as the angle increases.
- Deeper and longer defects in pipes lead to more substantial reductions in failure pressure.
- The developed ANN accurately predicts failure pressures in corroded pipes, aiding in quantifying and managing the risk of failure.

Keywords Artificial neural network · Corrosion · Finite element method · Pipe bend failure pressure · Pipeline integrity assessment

Abbreviations

ANN	Artificial Neural Network
ASME	American Society of Mechanical Engineers
DNV	Det Norske Veritas
FE	Finite Element
FEA	Finite Element Analysis

✉ Suria Devi Vijaya Kumar, suria_22000156@utp.edu.my | [1]Mechanical Engineering Department, Universiti Teknologi PETRONAS, 32610 Seri Iskandar, Malaysia. [2]College of Engineering, Birmingham City University, Birmingham B4 7XG, UK.

FEM	Finite Element Method
FFNN	Feed Forward Neural Networks
MPT	Magnetic particle testing
NDE	Non-destructive evaluation
RT	Radiographic testing
UT	Ultrasonic testing

List of symbols

D	Diameter of pipe
LF	Lorenz Factor
d	Depth of defect
l	Neuron in a hidden layer of artificial neural network
i	Input variable of artificial neural network
i_n	Normalised input variable of artificial neural network
l	Length of defect
o	Output variable of artificial neural network
P_f	Failure pressure of a corroded pipe elbow
P_i	Intact pressure of a pipe elbow
R	Bend radius of pipe elbow
R_b	Bend radius of pipe
R_m	Mean elbow radius
s_c	Circumferential defect spacing
s_l	Longitudinal defect spacing
t	Pipe wall thickness
UTS	Ultimate tensile strength
w	Defect width
y	Expected output of an ANN
α	Pipe bend angle
UTS^*	True ultimate tensile strength
σ_c	Axial compressive stress
σ_y	Yield stress
θ	Location of defect

1 Introduction

Pipelines hold immense significance within the oil and gas industry, serving as the lifeline for the efficient and safe transportation of hydrocarbon resources across vast and often challenging terrains. These pipelines are the backbone of the energy sector, facilitating the smooth flow of crude oil and natural gas from extraction points to processing facilities, distribution networks, and end-users who rely on these essential energy sources. The efficiency and safety of these pipelines are paramount, as any failure can result in environmental hazards, financial losses, and disruptions in energy supply.

High-Strength-Steel (HSS) pipelines represent a significant advancement in material technology, offering enhanced properties that make them highly suitable for the demanding environment of the oil and gas industry [1, 2]. These pipelines are characterized by their exceptional mechanical properties, including high tensile strength and toughness, which enable them to withstand extreme internal pressures and external forces, contributing to the efficiency and safety of hydrocarbon transportation [3–5]. Among the common material grades used in the industry are API 5L X70 to API 5L X100 [6].

In a pipeline system, pipe elbows stand out as potential weak links[7]. Pipe elbows are essential components used for routing pipelines and accommodating changes in direction. The geometry of these bends, defined by parameters such as the bend radius and angle, exerts significant influence over how the pipeline responds to internal pressure and axial compressive stress [8]. The critical factor contributing to the vulnerability of pipe elbows is the Bourdon effect, which result in stress concentrations that can lead to failure [9]. The Bourdon effect, associated with pipe bends,

amplifies the stress levels within the bend due to the curvature of the pipe. This effect can result in localized stress concentrations, making pipe elbows more susceptible to failure when subjected to internal pressure.

In addition, the integrity of the component is greatly compromised in the presence of corrosion defects. Corrosion poses a significant threat to pipelines, especially in the form of pitting corrosion. Corrosion is a well-documented issue in the industry, with pipelines traversing environments laden with corrosive substances that gradually erode the structural integrity of the steel [10]. Pitting corrosion, in particular, manifests as small, localized cavities on the pipeline's surface, compromising its mechanical properties and ultimately leading to failure if left unchecked [11].

Furthermore, the difference in surface areas between the intrados (inner) and extrados (outer) regions of the bend intensifies stress gradients, further complicating the structural response of pipe elbows to applied loads [9]. The influence of the location of defect on the residual strength of a pipe elbow, can be quantified by the Lorenz Factor (LF) derived by Bubenik and Rosenfeld in 1993 [12]. Based on their study, for a corrosion defect at the intrados, crown, and extrados, the LF is reduced to 1.25, 1.00, and 0.875, respectively, as represented by Eqs. 1–3. Based on these factors, it is evident that the intrados is the most critical part of the component, followed by the crown and extrados. Hence, it is crucial that the defects are detected and assessed to prevent catastrophic failures.

$$LF = \left[\frac{\frac{R_b}{R_m} - 0.5}{\frac{R_b}{R_m} - 1.0}\right] = 1.250 \tag{1}$$

$$LF = \left[\frac{\frac{R_b}{R_m}}{\frac{R_b}{R_m}}\right] = 1.000 \tag{2}$$

$$LF = \left[\frac{\frac{R_b}{R_m} + 0.5}{\frac{R_b}{R_m} + 1.0}\right] = 0.875 \tag{3}$$

In an incident in Alberta, Canada, an 8-inch pipeline operated by NOVA Gas Transmission Ltd. ruptured and ignited due to external corrosion, resulting in a substantial release of natural gas and a subsequent fire [13]. This incident demonstrates the global impact of corrosion-related pipeline failures, emphasizing the significance of employing non-destructive assessment methods for proper characterization of corrosion defects prior to residual strength assessment [14]. Non-destructive methods, such as ultrasonic testing (UT), play a crucial role in early detection and characterization of corrosion defects.

The integrity assessment of pipelines is a critical aspect of ensuring the safe and efficient transportation of hydrocarbon resources. Muthanna et al. [15] conducted an assessment of corroded API 5L X52 pipe elbows using a modified failure assessment diagram. Their study highlights the importance of understanding the structural integrity of pipelines in corrosive environments. Similarly, Shuai et al. [16] developed an empirical model to predict the burst pressure of corroded elbows using finite element modelling. These studies underscore the significance of accurately assessing corrosion-induced degradation to prevent catastrophic failures in pipelines.

Failure analysis is another crucial aspect in pipeline integrity management. Zhou et al. [4] utilized finite element analysis to examine the failure of high-strength steel pipelines with group corrosion defects, shedding light on the failure mechanisms under complex corrosion scenarios. Arumugam et al. [8] conducted a review on the influence of axial compressive stress and internal pressure on pipeline networks, underscoring the importance of considering mechanical stress effects in pipeline design and integrity assessment processes.

In the context of corrosion assessment, established codes and standards exist for straight pipes, such as DNV-RP-F101 and ASME B31G, which provide comprehensive frameworks for evaluating the integrity of straight sections of pipelines [17, 18]. However, when it comes to pipe elbows, there is a notable absence of specific codes and guidelines for assessing their structural integrity, despite their critical role in pipeline systems. This gap in industry standards underscores the complexity of evaluating the combined influence of bend parameters, corrosion defects, and the applied loads on pipe elbows [8].

To address these challenges, numerical analysis, particularly using the Finite Element Method (FEM), emerges as a powerful tool for assessing the structural response of pipeline components to various loads such as internal pressure

Table 1 Overview of geometric parameters and materials used

Parameter	Value(s)
Diameter of pipe, D	300 mm
Pipe wall thickness, t	10 mm
Defect location (θ)	−90°, 90°
Pipe bend angle, α	30°, 45°, 90°
Normalized pipe elbow bend radius, R/D	2.5, 3.5, 4.5
Normalized defect width, w/t	10
Normalized defect depth, d/t	0.0, 0.2, 0.4, 0.6, 0.8
Normalized defect length, l/D	0.0, 0.2, 0.5, 0.8, 1.1, 1.4
Normalized defect spacing, $s/\sqrt{Dt}$	0.0, 0.5, 1.0, 2.0
Normalized axial compressive stress, σ_c/σ_y	0.0, 0.2, 0.4, 0.6, 0.8
Pipe grades	API 5L X70, X80 and X100

and axial compressive stress [19, 20]. FEM allows for the prediction of stress distribution, deformation, and potential failure modes, aiding in the assessment of the remaining strength of these components. Nevertheless, the accuracy and reliability of FEM results are contingent on precise input parameters, including material properties and defect geometries, which are often obtained through experimental testing.

The manuscript begins with an introduction to the study's objectives and the importance of understanding the effects of corrosion and pipe geometry on failure pressures. Following this, the paper details the methodology, including data preparation, network architecture, training procedure, and performance metrics. Results and discussions are presented, covering the impact of pipe bend geometry, defect characteristics, and axial compressive stress on failure pressures. The development and validation of the Artificial Neural Network (ANN) are then described, followed by the conclusion summarizing key findings and implications.

2 Methodology

2.1 Overview of geometric parameters and materials

This study involves an investigation into the influence of various geometric parameters on the behaviour of high-strength steel pipes, summarized in Table 1. The pipe diameter, pipe wall thickness, and defect width were fixed at 300 mm, 10 mm, and 100 mm, respectively. The investigated parameters were the pipe bend angle (α = 30°, 45°, 90°), normalized bend radius (R/D: 2.5, 3.5, 4.5), normalized defect depth (d/t: 0.0 to 0.8), normalized defect length (l/D: 0.0 to 1.4), normalized defect spacing ($s/\sqrt{Dt}$: 0.0 to2.0), and defect location (θ: -90°, 90°) [7, 16, 21–24]. Additionally, the study considered normalized axial compressive stress (σ_c/σ_y) values ranging from 0.0 to 0.8, to comprehensively explore how these parameters interact. Figure 1 illustrates the quarter models of the corroded pipes used in this study. The corrosion defects are modelled on the external surface of the pipe.

For the material, API 5L X70, API 5L X80, and API 5L X100 are considered, along with endplate material specifications, summarised in Table 2. These properties include the modulus of elasticity (E) of 210 GPa, a Poisson's ratio (v) of 0.3, true ultimate tensile strength (UTS^*) values of 606.72 MPa, 754.56 MPa, and 890.88 MPa, and yield stress (σ_y) values of 516.48 MPa, 570.80 MPa, and 652.80 MPa for API 5L X70, API 5L X80, and API 5L X100, respectively. The endplate material exhibits a substantially higher modulus of elasticity at 210,000 GPa [25]. Figure 2 presents the true stress–strain curve of these materials, offering a visual representation of their mechanical behavior under load.

2.2 Development of finite element method

2.2.1 Material modeling

A comprehensive material characterization was carried out to accurately simulate the structural behaviour of these high-strength steel pipes based on their respective material properties, such as modulus of elasticity, Poisson's ratio, true

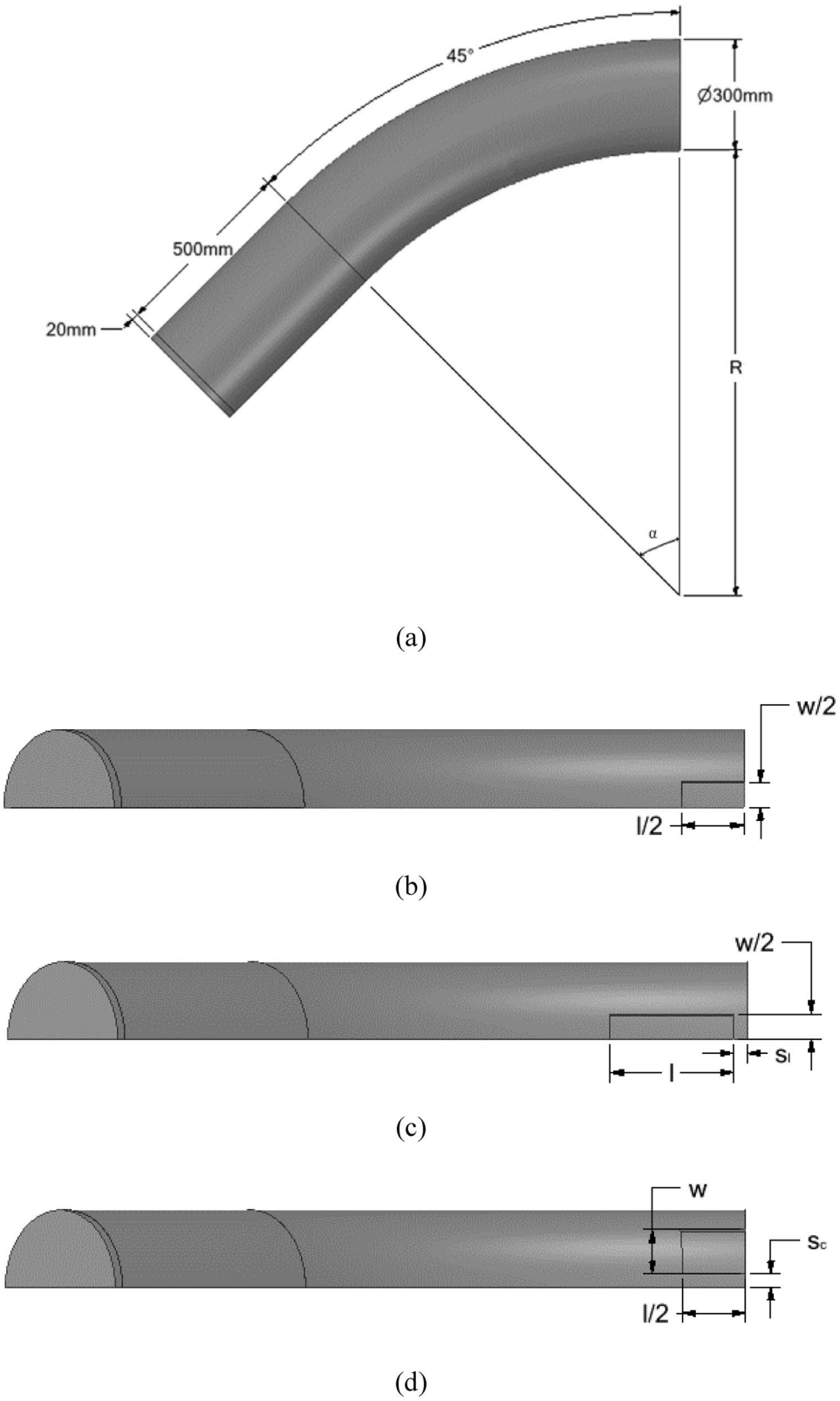

Fig. 1 Quarter model of a pipe elbow with **a** no defects **b** a single defect **c** longitudinal interacting defects **d** circumferential interacting defects

Table 2 Mechanical properties of the materials used in the study [26, 27]

Property	Value			
	API 5L X70	API 5L X80	API 5L X100	Endplate
Modulus of elasticity, *E* (GPa)	210	210	210	210,000
Poisson's ratio,*v*	0.3			
True ultimate tensile strength, *UTS** (MPa)	606.72	754.56	890.88	–
Yield stress, σ_y (MPa)	516.48	570.8	652.8	–

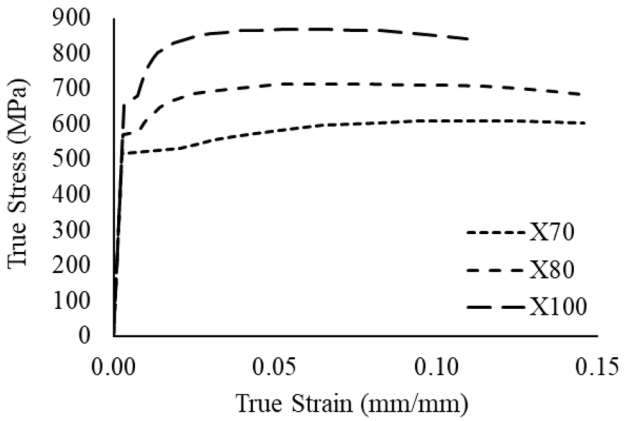

Fig. 2 True stress strain curve of the materials used in this study [26, 27]

ultimate tensile strength, and yield stress. The material was assumed to be homogenous. The incorporation of endplates and the utilization of a quarter model allowed for computational efficiency while maintaining an accurate representation of the real-world conditions. This approach ensured that the material behaviour, when subjected to the specified loading conditions, was accurately captured within the finite element analysis. As for the shape of defect, a rectangular defect idealization was used in this study.

2.2.2 Mesh generation

The pipe body was discretized using solid quadrilateral elements, ensuring accurate representation of the geometry's intricacies. To capture the critical details of corrosion defects, a mesh size of 2 mm with a minimum of 3 layers was employed in the defect region. A bias with an aspect ratio of 0.5 was introduced away from this region, facilitating a gradual transition in mesh density. Additionally, the endplate was meshed using solid triangles with a uniform mesh size of 10 mm. These meshing strategies aimed to balance computational efficiency and precision in simulating the pipe's structural response. Figure 3 illustrates the fully meshed component of the quarter models for a corroded pipe with a single defect, longitudinally aligned interacting defects, and circumferentially aligned interacting defects. The magnification of the meshed corrosion defect region is provided in Fig. 4.

2.2.3 Boundary conditions

As illustrated in Fig. 5, symmetry boundary conditions were employed to reduce computational complexity while maintaining accuracy. Internal pressure was incrementally applied to the inner surface of the pipe wall, to replicate gradual real-world loading conditions. Similarly, axial compressive stress was incrementally introduced at the endplate's outer surface, emulating the effects of axial forces. These loading conditions were applied in two distinct timesteps at isothermal conditions to capture the dynamic response of the pipes. Constraints on the degrees of freedom (DOF) were implemented in the x, y, and z axes to maintain structural stability and prevent unintended movement. These constraints were applied at the center of the outer surface of the endplate, effectively immobilizing any rotation or translation in

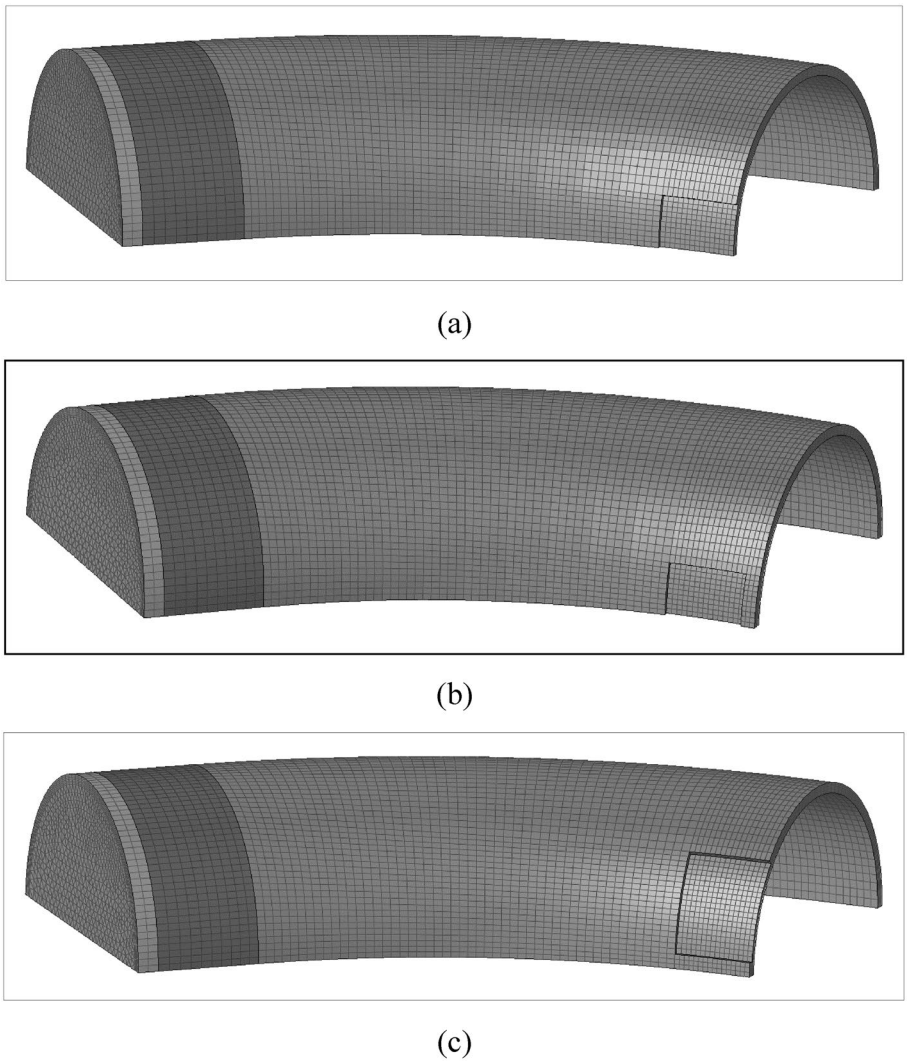

Fig. 3 Meshed quarter models of a corroded pipe with **a** a single defect, **b** longitudinally aligned interacting defects, **c** and circumferentially aligned interacting defects

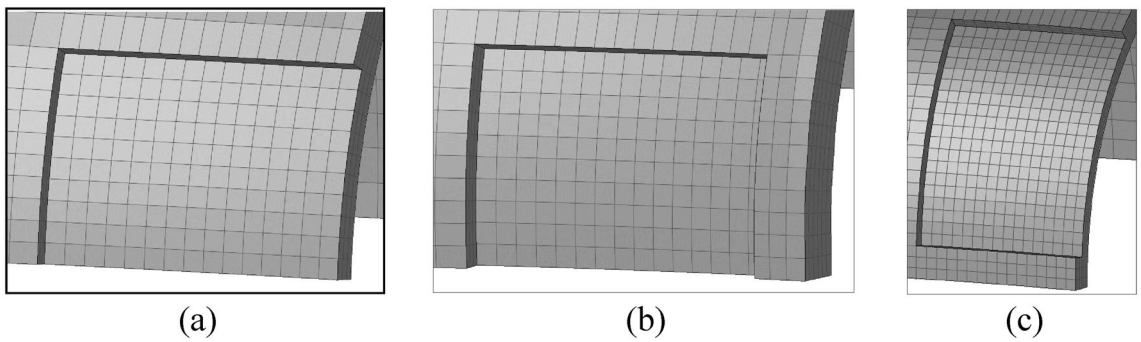

Fig. 4 Magnification of the corrosion defect region for a meshed pipe with corrosion defect region for a pipe with **a** a single defect, **b** longitudinally aligned interacting defects, **c** and circumferentially aligned interacting defects

those directions. These boundary conditions were carefully designed to mirror real-world conditions and enhance the accuracy of the finite element analysis.

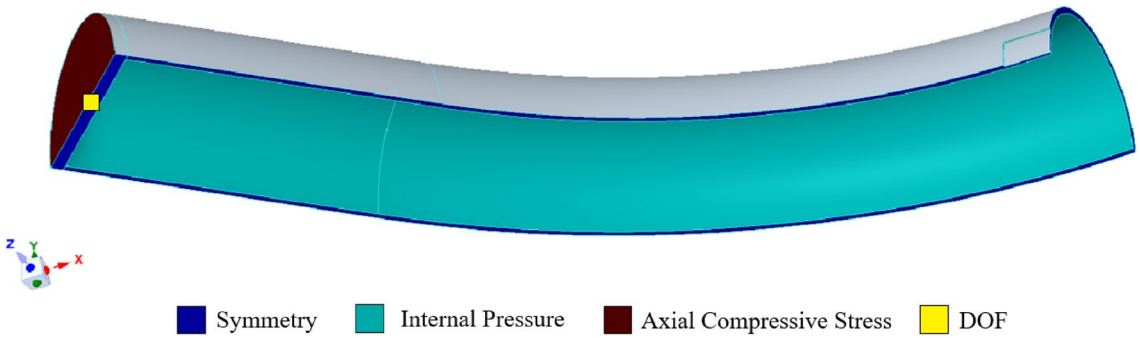

Fig. 5 Application of boundary conditions on the quarter pipe model

Table 3 Results of the validation study

Author, Year	Shuai et al. [16]	Benjamin et al. [28]
Pipe type	Elbow	Straight
Analysis type	FEM	Burst test
Material	X80	X80
Specimen	Convergence test model	IDTS 4
Burst Pressure (MPa)	30.6	21.14
FEA failure pressure (MPa)	29.74	20.62
Percentage Difference (%)	− 2.81	− 2.46

2.2.4 Failure criterion

The von Mises stress-based criterion served as the measurement metric for evaluating the structural performance of the high-strength steel pipes. The criterion defined the point at which a pipe was deemed to have failed, and this occurred when the von Mises stress reached the true ultimate tensile stress (UTS). Failure pressure was determined based on the specific timestep at which failure occurred to ensure a precise and accurate assessment of the pipes' failure behaviour.

2.2.5 Validation of the finite element method

Two sources, Shuai et al. [16] and Benjamin et al. [28], were considered for the validation study, as listed on Table 3. Shuai et al. conducted FEM analysis on an elbow pipe made of X80 material, while Benjamin et al. performed a burst test on a straight pipe of the same material. The FEA-derived failure pressures for the elbow pipe and straight pipe in this study showed remarkable agreement with the experimental results, with a percentage difference of -2.81% and -2.46%, respectively. This close alignment between the FEA predictions and experimental data, underscoring the validity and reliability of the FEM employed in the current study.

2.3 Development of artificial neural network

2.3.1 Data preparation

A total of 21,601 datasets were generated through FEM simulations, taking into account various geometric parameters (see Table 1). The failure pressures obtained from these simulations were normalized to the failure pressure of the pristine pipe. This dataset was used for the training of the ANN.

2.3.2 Network architecture

The ANN employed in this study was designed to capture the relationships between input parameters and the normalized failure pressure of corroded pipes. The ANN consisted of nine input nodes, representing the true ultimate tensile strength of the pipe, normalized pipe elbow bend radius, pipe bend angle, defect location, normalized defect depth, normalized defect length, normalized longitudinal and circumferential defect spacing, and normalized axial compressive stress. The ANN featured two hidden layers, with the first hidden layer comprising eight neurons and the second hidden layer housing six neurons. These hidden layers allowed the network to represent complex patterns in the data. The ANN's output layer comprised a single node for predicting corresponding to the normalized failure pressure of the corroded pipe. This architecture enabled the ANN to learn and generalize from the data set to predict failure pressures under varying conditions.

2.3.3 Training procedure

The Levenberg Marquardt back-propagation algorithm is a variant of the classic back-propagation algorithm, renowned for its effectiveness in training artificial neural networks (ANNs). Unlike traditional gradient descent methods, Levenberg Marquardt combines the advantages of both the steepest descent and Gauss–Newton algorithms. It adjusts the learning rate dynamically during training, allowing for faster convergence and improved stability.

In the context of the provided scenario, the algorithm was utilized to train the ANN on a carefully partitioned dataset. The dataset was split into three subsets: a training set comprising 70% of the data, a testing set containing 15%, and a validation set with another 15%. This division is crucial for ensuring the model's ability to generalize well to unseen data. During training, the Levenberg Marquardt algorithm optimizes the network's parameters by iteratively adjusting them based on the error between the predicted outputs and the actual targets, utilizing information from the training data.

2.3.4 Performance metrics

The performance metrics used in the assessment of the ANN are the Mean Squared Error (MSE) and R-squared (R^2) regression analysis. The MSE was used to identify the epoch with the lowest MSE. Additionally, R-squared regression analysis was applied to gauge the goodness-of-fit between the ANN predictions and the actual data. These performance metrics collectively ensured a robust evaluation of the ANN's accuracy and predictive capabilities based on the weights and biases of the ANN.

2.3.5 Validation of the artificial neural network

The validation procedures for the developed ANN involved a rigorous assessment of its predictive capabilities using previously unseen data. A separate and arbitrary dataset was generated using FEM, constituting a total of 30 new datasets to ensure an unbiased evaluation. Importantly, these datasets were not introduced to the ANN during the training phase, ensuring the network was tested on entirely unseen data. This approach provided a robust validation process, verifying the ANN's ability to generalize and accurately predict the normalized failure pressures of corroded pipes under diverse conditions. The utilization of this distinct dataset for validation and testing underscored the network's reliability and its capacity to make meaningful predictions beyond the scope of the training data.

3 Results and discussion

3.1 Effect of pipe bend geometry and defect orientation on failure pressure

3.1.1 Pipe bend angle and defect orientation

Figure 6 illustrates the failure pressures of API 5L X70 pipe bends subjected to internal pressure and axial compressive stress. In this case, pristine pipe bends, pipe bends with a single defect ($d/t = 0.2, l/D = 0.8$), as well as pipe bends with longitudinally and circumferentially interacting corrosion defects ($d/t = 0.2, l/D = 0.8, s/\sqrt{Dt} = 0.5$) located at the intrados is used.

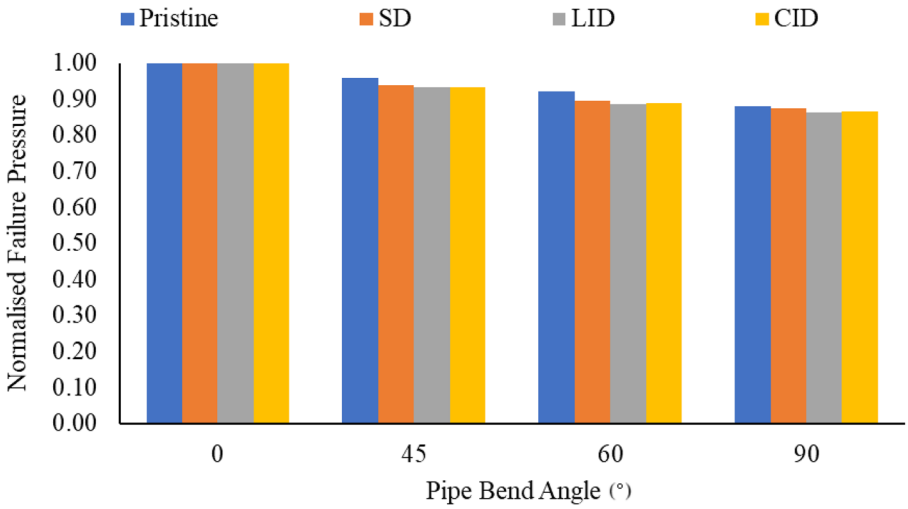

Fig. 6 Normalised failure pressures of API 5L X70 pipe bends subjected to combined loadings for increasing values of pipe angles

The analysis (Fig. 6) shows that the failure pressure of pipe bends decreases as the bend angle increases for both pristine and corroded conditions. For defect-free (pristine) pipes, failure pressure drops from 100 to 88%, as the bend angle increases from 0 to 90 degrees. The failure pressure of pipes with a single corrosion defect (SD) drop from 100 to 94% at a 45-degree bend. The failure pressure of pipes with longitudinally aligned interacting corrosion defects (LID) shows a more pronounced decrease, from 100 to 86% between 0 and 90 degrees. Circumferentially aligned interacting corrosion defects (CID) result in a similar trend, with failure pressure decreasing from 100 to 87% as the bend angle goes from 0 to 90 degrees. This is consistent with the findings of Mondal et al. in 2022, where the effect of bend angle on the failure pressure of pipe bends subjected to internal pressure only was studied [7]. In the presence of axial compressive stress, the decrease in failure pressure is more significant, especially for pipe bends with corrosion defects of greater depth and length.

An increase in the bend angle of a pipe increases the stress concentration, particularly at the intrados, which is the most vulnerable point due to bending. This stress concentration is exacerbated as the angle increases, leading to a reduction in the failure pressure. Essentially, the pipe experiences a more significant distortion due to the bending moment at the intrados, making it the weakest link in the pipe. As the angle becomes more acute, the pipe's ability to withstand internal pressure without failing is reduced, hence the observed decrease in failure pressure with increased bend angle.

Pipes with a single defect show a slight decrease (2.5% to 3.0%) in failure pressure compared to pristine ones. The presence of corrosion defects inherently weakens the structural integrity of pipe bends. The pressure drop is more significant for pipes with longitudinally and circumferentially aligned interacting defects (13% to 15%), indicating that the orientation of defects has a considerable impact on the structural integrity of pipe bends. Single defects slightly reduce the failure pressure as they interrupt the uniform stress distribution within the pipe material. The situation is exacerbated when defects are aligned longitudinally or circumferentially, as these configurations can create overlap regions of stress concentration that significantly compromise the pipe's ability to withstand internal pressures. The differences in failure pressure of longitudinally and circumferentially aligned corrosion defects were minimal, ranging from 0.3% to 1.0%, for similar defect geometries.

3.1.2 Pipe bend radius

Figure 7 depict the influence of pipe bending radius on the failure pressure at different pipe locations. In this analysis, 90° pipe bends with a single corrosion defect ($d/t = 0.2, l/D = 0.8$) located at the intrados is used. Notably, for defects located at the intrados, an increase in bending radius from 2.5D to 4.5D bending radius yields a marginal increase in normalized failure pressure, rising from 0.88 to 0.91. Conversely, defects at the extrados exhibit a more significant response. The normalized failure pressure decreases from 0.98 at a 2.5 D bending radius to 0.93 at a 4.5 D bending radius, suggesting that the failure pressure at the extrados is more sensitive to changes in the pipe bending radius than at the intrados. The intrados is subjected to tension and undergoes elongation. Conversely, the extrados is subjected to compressive stress where material compression occurs. The failure pressure of the pipe depends on these stress patterns, and changes in the

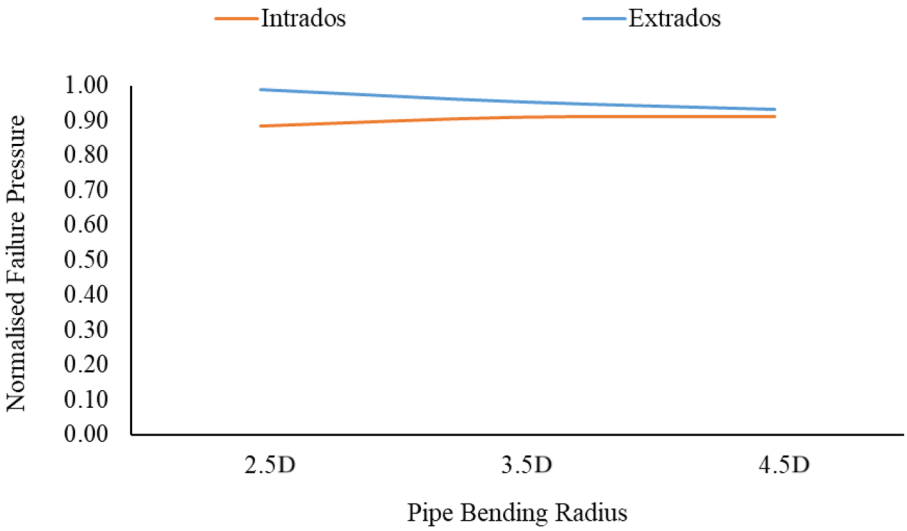

Fig. 7 Normalised failure pressures of API 5L X70 pipe bends subjected to combined loadings for increasing values of pipe bending radii

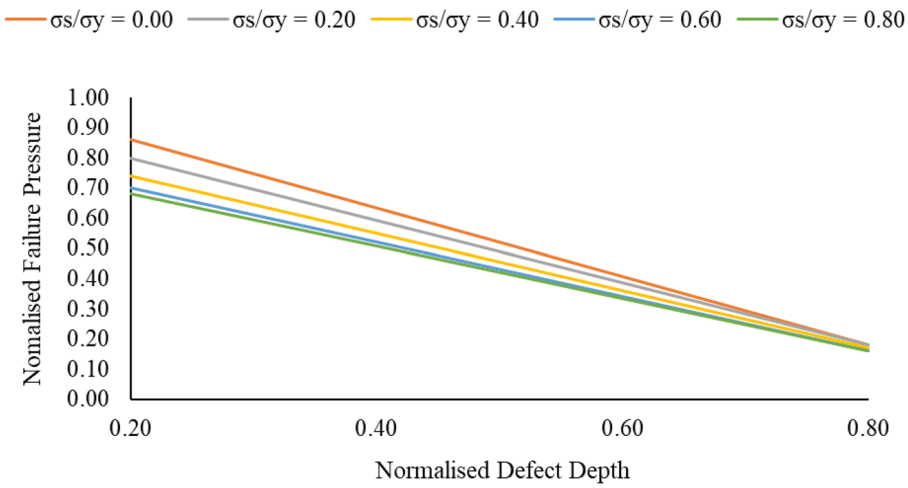

Fig. 8 Normalised failure pressures of API 5L X70 pipe bends subjected to combined loadings for increasing values of normalized defect depths

bending radius directly affect the stress magnitude. An increased bending radius contributes to a more uniform stress distribution, potentially increasing the failure pressure as it reduces the concentration of stress at any singular point.

3.2 Effect of corrosion defect characteristics on failure pressure

3.2.1 Defect depth

Figure 8 illustrates a linear decrease in normalized failure pressure with an increase in normalized defect depth for varying ratios of axial compressive stress. An API 5L X70 90° pipe bend with a single defect ($l/D = 0.8$) located at the intrados is analysed. The failure pressure decreases from near 0.95 to 0.19 as the defect depth increases from 0.20 to 0.80. This trend is consistent across all stress ratios from 0.00 to 0.80. A more pronounced reduction in failure pressure is observed as the operational stress approaches the material's yield stress, as the normalized defect depth increases, the pipe's cross-sectional area capable of withstanding stress diminishes. This reduction in the effective load-bearing area decreases the capacity to resist internal pressures without yielding or fracturing. Moreover, when the applied stress approaches the yield stress, the material is closer to its elastic limit and defects become more critical, with a reduced margin of safety.

3.2.2 Defect length

Figure 9 displays the relationship between normalized defect length and normalized failure pressure of API 5L X70 90°pipe bends for different defect depth ratios. A pipe bend with a single defect located at the intrados subjected to

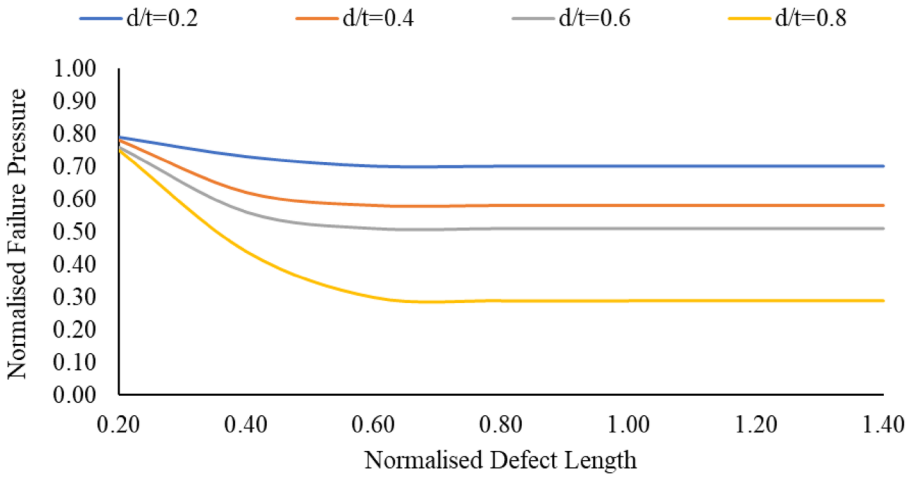

Fig. 9 Normalised failure pressure of an API 5L X70 pipe elbow subjected to combined loadings for increasing values of normalised defect lengths

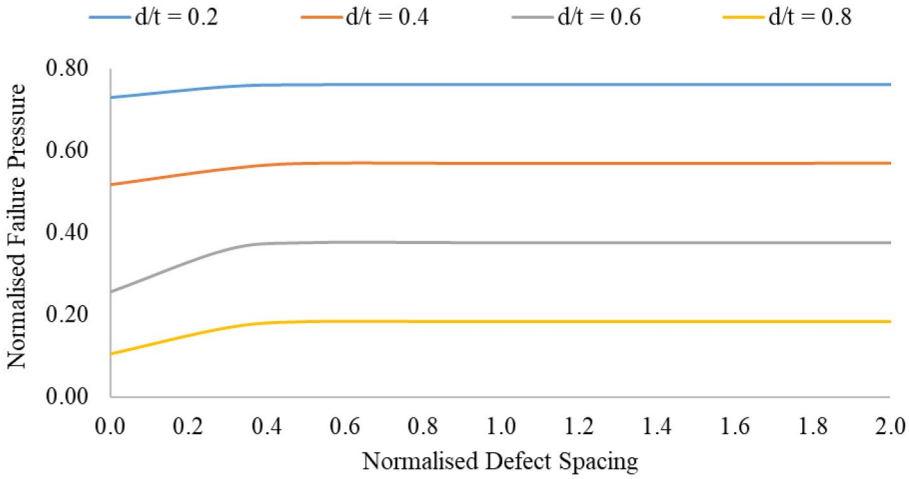

Fig. 10 Normalized failure pressure of an API 5L X70 pipe elbow subjected to combined loadings for increasing values of normalized defect spacings (longitudinal)

internal pressure and axial compressive stress is analyzed. As the defect length increases, the failure pressure decreases significantly for all depth ratios (ranging from 11.5% to 48.2%) with the greatest reduction observed for a normalized defect depth of 0.80 due to the extent the pipe wall was compromised by the defect. A longer defect spans a wider area, reducing the pipe's ability to contain internal pressures. This effect is more pronounced for deeper defects (d/t > 0.4), as there is less remaining wall thickness to resist the pressure, leading to a steeper decline in failure pressure.

Beyond a normalized defect length of 0.80, the failure pressure begins to plateau, resulting in an insignificant change in failure pressure (< 0.5%) beyond this critical point (l/D = 0.80). The plateauing of failure pressure beyond a normalized defect length of 0.80 indicates that the pipe's capacity to withstand internal pressure has reached a critical threshold where the additional defect length does not significantly compromise the structure further. This suggests that the length of the defect no longer influences the pipe's integrity, as the critical stress area has been maximally affected by the existing defect.

3.2.3 Defect spacing

In this case, API 5L X70 90° pipe bend with defects of $d/t = 0.6$, $l/D = 0.8$ and $s/\sqrt{Dt} = 0.5$ aligned longitudinally and circumferentially located at the intrados is analysed. For longitudinally aligned interacting corrosion defects (Fig. 10), the impact on failure pressure becomes less pronounced as defect spacing increases, particularly for shallow defects. For a normalized defect depth of 0.2 and 0.4 (shallow defects), the failure pressure increases by 8.6% and 9.7%, respectively, as defect spacing increases. In contrast, deeper defects ($d/t = 0.6$ and 0.8) show a significant increase in failure pressure, ranging from 25.6% to 36.4% indicating that when defects are deep ($d/t > 0.4$), the spacing between them has

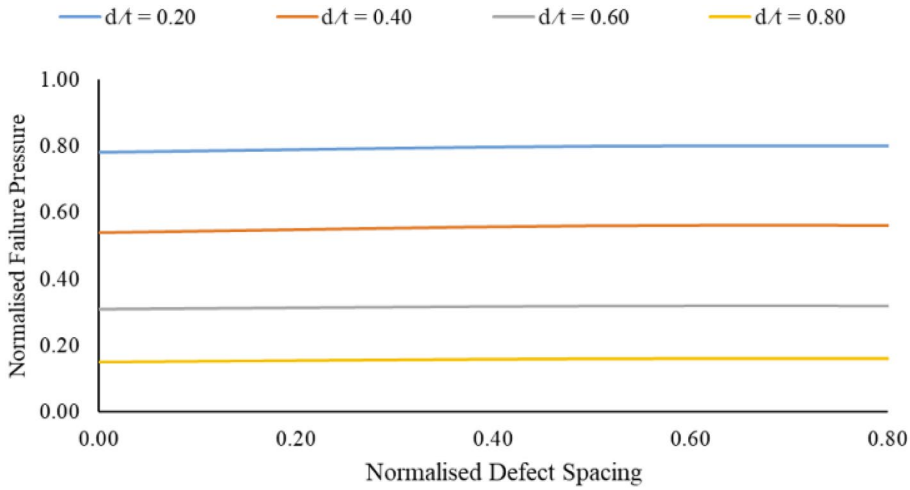

Fig. 11 Normalised failure pressure of an API 5L X70 pipe elbow subjected to combined loadings for increasing values of normalised defect spacings (circumferential)

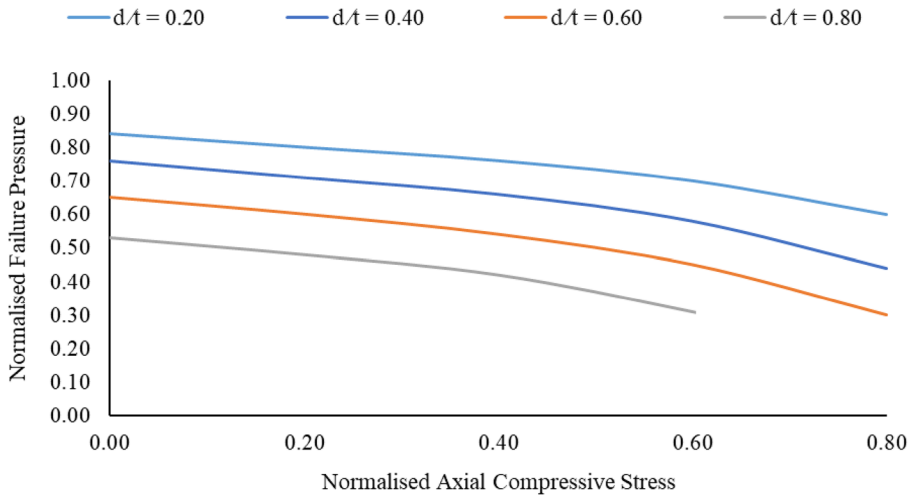

Fig. 12 Normalised failure pressure of an API 5L X70 pipe elbow subjected to combined loadings

a significant effect on the failure pressure. The interaction among defects is more pronounced with deeper and larger defects due to the greater reduction in the effective wall thickness and the overlap of stressed regions around each defect.

An increase in defect spacing insignificantly influenced the failure pressure of the pipe bend for circumferentially aligned interacting corrosion defects, as illustrated in Fig. 11. The maximum increase in failure pressure was only 1.29% for a normalized defect depth of 0.2. This minimal impact implies that the failure pressure of pipes with circumferentially aligned defects is primarily determined by other factors, such as the length and depth of the defects, rather than the spacing between them.

3.3 Combined effects of axial compressive stress

Figure 12 shows the normalized failure pressure as a function of normalized axial compressive stress for various normalized defect depth ratios. The failure pressure consistently decreases across all defect depth ratios as the axial compressive stress increases. For shallower defects ($d/t < 0.40$), the failure pressure decreases gradually with a maximum reduction of 17.4%. In contrast, deeper defects ($d/t > 0.40$) exhibit a more marked decrease in failure pressure (> 20%) as axial compressive stress increases, indicating that pipes with deeper defects are more susceptible to axial compressive loads. For normalised defect defects of greater than 0.60, buckling occurs when subjected to a normalized axial compressive stress of greater than 0.60.

When compared with straight pipes from a study by Vijaya Kumar et al. 2022, it was observed that in pipe elbows, even a small ratio of compressive stress results in a significant reduction of failure pressure, unlike in straight pipes where a significant influence is observed for normalized axial compressive stress values of more than 0.4 [29], indicating that

pipe elbows with defects have a lower tolerance for axial compression before yielding or failing and underscoring the importance of considering compressive stresses in their assessment and design.

3.4 Development of empirical equation for failure pressure prediction of corroded pipes

An empirical equation for predicting the failure pressure of corroded pipe bends was developed using an ANN. The inputs of the ANN are the true ultimate tensile strength of the pipe, pipe bend angle, pipe bending radius, defect location, normalized defect depth, length, longitudinal and circumferential spacing, and axial compressive stress. A substantial dataset of 14,403 points, generated via FEM, was used to train the ANN. The flow of the ANN training is illustrated in Fig. 13, while the developed ANN architecture is illustrated in Fig. 14.

The regression analysis of the ANN developed for predicting pipe bend failure pressure demonstrates exceptional performance across all data subsets. The coefficient of determination (R^2) is consistently high at 0.99 for training, validation, and test phases, indicating a near-perfect fit between the predicted values and the actual data. The Mean Squared Error (MSE), a measure of prediction accuracy, is low, with values of 0.000654 for training, 0.000335 for validation, and 0.000634 for the test set, further confirming the ANN's robust predictive capability.

The ANN was further validated using a separate FEM-generated dataset. It comprised 30 datasets each for defects at the intrados and extrados. The model achieved a minimum and maximum difference of -5.29% and 3.42% respectively, with a standard deviation of 1.93. All percentage differences were within four standard deviations of the mean. As such, the likelihood of encountering an error exceeding 7.72% was calculated to be 1 in 15,787, underscoring the model's high accuracy and reliability.

Based on the matrix representation of the developed ANN, the empirical equation to predict the failure pressure of a corroded pipe bend subjected to internal pressure and axial compressive stress was formulated (Eqs. 4–6). The normalized input values can be calculated using Eqs. 7–16. This empirical solution is applicable for corroded pipe bends with a single or interacting defect located at the intrados or extrados of a pipe bend subjected to internal pressure and normalized axial compressive stress ranging from 0.0 to 0.8, with a bend angle ranging from 30° to 90°, normalized bending radius between 2.5 to 4.5, normalized defect depth of 0.0 to 0.8, normalized defect length of 0.0 to 1.4, normalized longitudinal and circumferential defect spacing of 0.0 to 2.0, and true ultimate tensile strength ranges of 606.72 MPa to 890.88 MPa.

$$\begin{bmatrix} I_{1,1} \\ I_{1,2} \\ I_{1,3} \\ I_{1,4} \\ I_{1,5} \\ I_{1,6} \\ I_{1,7} \\ I_{1,8} \end{bmatrix} = \begin{bmatrix} 0.0026 & 0.0078 & -0.0550 & 0.0195 & -0.0222 & 0.0069 & 0.0145 & -0.0030 & 1.2598 \\ 0.0008 & -0.0052 & 0.3221 & 0.5367 & -0.0144 & -0.0070 & -0.0103 & -0.0002 & -0.0413 \\ 0.0756 & -0.0312 & -0.0352 & -0.0099 & -1.0976 & 5.2522 & 0.2891 & 0.0015 & -0.0079 \\ 0.1510 & -0.0131 & -0.0061 & -0.0071 & -0.0933 & 0.2199 & -6.5074 & 0.0049 & -0.0035 \\ 0.0410 & 0.0018 & 0.1072 & -0.0203 & 7.3867 & -0.0578 & -0.0093 & 0.0362 & -0.2674 \\ 0.0610 & -0.0639 & 0.0062 & 0.0023 & 0.1611 & -0.0973 & 2.1833 & 7.0263 & 0.0038 \\ 2.8805 & -5.0509 & -0.3562 & -0.0126 & -23.8101 & -9.9916 & 0.6190 & -2.3353 & -0.0490 \\ -0.0049 & -0.0082 & -0.0122 & 0.0065 & -0.2405 & -0.0062 & -0.0159 & -0.0036 & -0.0153 \end{bmatrix} \begin{bmatrix} i_1 \\ i_2 \\ i_3 \\ i_4 \\ i_5 \\ i_6 \\ i_7 \\ i_8 \\ i_9 \end{bmatrix} + \begin{bmatrix} 1.6829 \\ 2.8774 \\ 3.3510 \\ -5.8752 \\ -1.9974 \\ 8.9784 \\ -14.5529 \\ 0.2987 \end{bmatrix} \tag{4}$$

$$\begin{bmatrix} I_{2,1} \\ I_{2,2} \\ I_{2,3} \\ I_{2,4} \\ I_{2,5} \\ I_{2,6} \end{bmatrix} = \begin{bmatrix} 0.7579 & 1.8633 & 2.6590 & 0.7146 & -1.1366 & 0.0513 & 3.4111 & -4.7741 \\ -0.0314 & 0.4865 & 0.0001 & -0.0167 & 0.0011 & -0.0118 & 0.0018 & 0.2635 \\ 18.5641 & -10.1670 & 0.2834 & -0.0814 & 2.4735 & 0.0258 & -0.6468 & 8.1774 \\ 0.0522 & 0.4680 & -0.0399 & 0.9091 & -0.0388 & 0.3760 & -0.0263 & -0.0897 \\ -0.0595 & 1.4800 & -20.6858 & 1.0055 & -0.3585 & 0.5682 & 0.1780 & 0.6456 \\ 0.0856 & -1.3634 & -0.2832 & 13.5154 & -0.2616 & 23.9340 & 0.2075 & 7.4657 \end{bmatrix} \begin{bmatrix} a(I_{1,1}) \\ a(I_{1,2}) \\ a(I_{1,3}) \\ a(I_{1,4}) \\ a(I_{1,5}) \\ a(I_{1,6}) \\ a(I_{1,7}) \\ a(I_{1,8}) \end{bmatrix} + \begin{bmatrix} -0.6750 \\ -0.6802 \\ -14.5998 \\ -1.2759 \\ -22.0008 \\ 3.6438 \end{bmatrix} \tag{5}$$

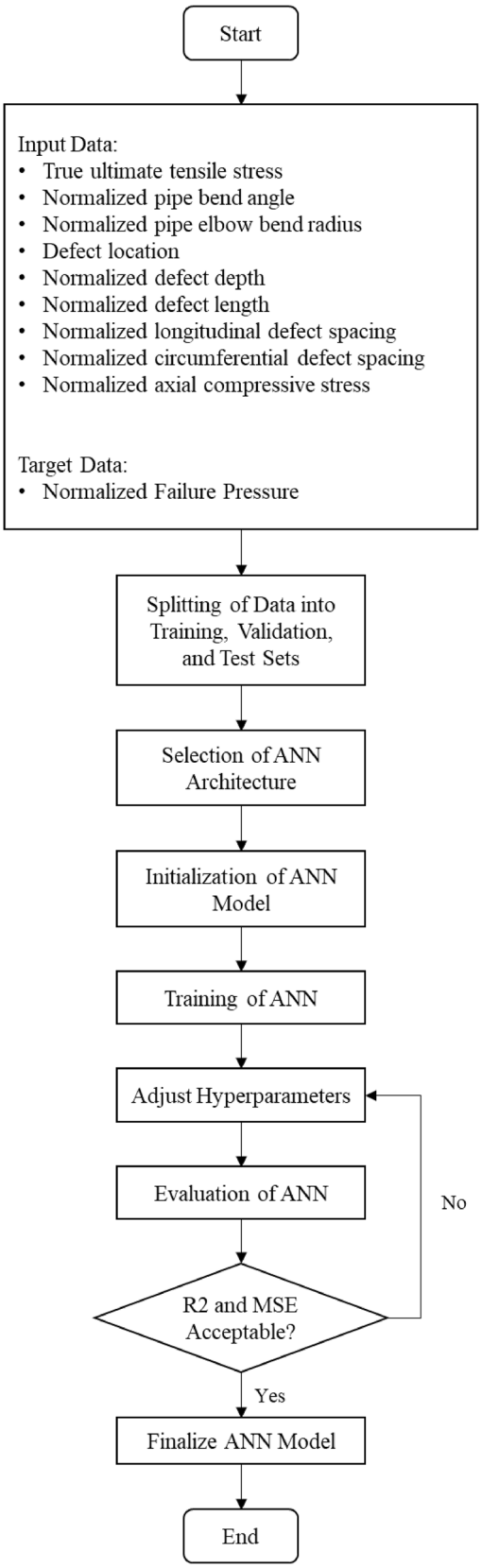

Fig. 13 Flow of the ANN algorithm

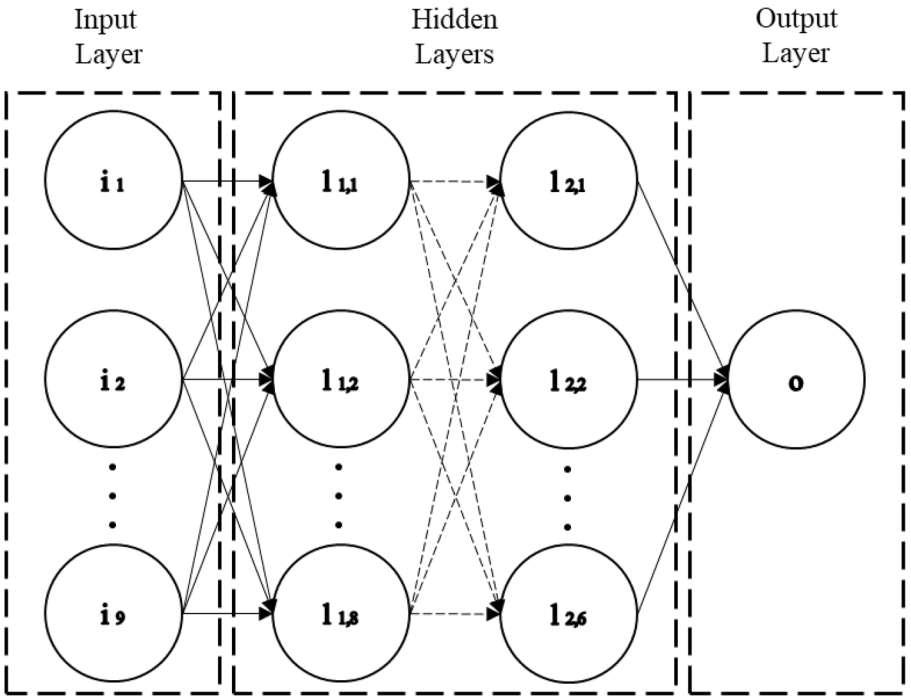

Fig. 14 Architecture of the developed ANN

$$\left[P_f\right] = P_i\left[0.41\left[\begin{bmatrix}-0.0168 & 10.7514 & 3.6467 & 0.3614 & 0.1400 & 9.5939\end{bmatrix}\begin{bmatrix}a(I_{2,1})\\ a(I_{2,2})\\ a(I_{2,3})\\ a(I_{2,4})\\ a(I_{2,5})\\ a(I_{2,6})\end{bmatrix} + [-0.32]\right] - 0.35\right] \tag{6}$$

where

$$a(x) = \frac{e^{2x}-1}{e^{2x}+1} \tag{7}$$

$$i_1 = \frac{x - 172710}{80656} - 1 \tag{8}$$

$$i_2 = \frac{\theta + 2070}{2025} - 1 \tag{9}$$

$$i_3 = \frac{-5\mathrm{D}^2 + \mathrm{R} - 2.5\mathrm{D}}{4D^2} - 1 \tag{10}$$

$$i_4 = \begin{cases} 0.0 \textit{ for defects located at the extrados;} \\ 0.5 \textit{ for defects located at the intrados.} \end{cases} \tag{11}$$

$$i_5 = \frac{5\left(\frac{d}{t} - 0.2\right)}{3} - 1$$

$$i_6 = \frac{5\left(\frac{l}{D} - 0.2\right)}{6} - 1 \tag{12}$$

$$i_7 = \frac{\left(s_l/\sqrt{Dt}\right)}{2} - 1$$

$$i_8 = \frac{\left(s_c/\sqrt{Dt}\right)}{2} - 1 \tag{13}$$

$$i_9 = \frac{5\left(\frac{\sigma_c}{\sigma_y}\right)}{4} - 1 \tag{14}$$

4 Conclusion

In conclusion, there is a clear correlation between bend angle and failure pressure, with a noticeable reduction in failure pressure as the bend angle increases. Pristine pipes experience a decrease to 88% for a 90 degrees bend radius, while pipes with corrosion defects exhibit even greater sensitivity to bend angle changes. Furthermore, the bending radius plays a significant role, especially for defects located at the extrados, where a larger radius leads to a more significant increase in normalized failure pressure, emphasizing the importance of considering pipe geometry when assessing structural integrity.

The study also highlights the critical impact of defect depth and length on failure pressure, with deeper and longer defects leading to more pronounced reductions. The spacing between defects becomes crucial, particularly for deeper defects, which experience substantial failure pressure increases with greater spacing. Additionally, the influence of axial compressive stress is evident, with deeper defects displaying heightened vulnerability to such loads, underscoring the necessity to consider axial compression in pipe bend design.

Finally, an empirical equation using an Artificial Neural Network with an R^2 value of 0.99 was developed, for the assessment and design of corroded pipe bends. With an extensive dataset of 14,403 points and robust performance metrics, this equation is a valuable tool for engineers seeking to quantify and mitigate the risk of failure in corroded pipe bends.

This study provides valuable insights into predicting failure pressures in corroded pipe bends, essential for ensuring structural integrity in various industries. By employing an Artificial Neural Network, it offers a robust predictive tool, aiding engineers in assessing and mitigating risks. Limitations include reliance on simulation data and assumptions about material behavior under load.

Future studies in this field could analyse the influence of temperature fluctuations on the failure pressure of corroded pipe bends, particularly in pipelines exposed to extreme environmental conditions. Additional defect types and configurations can be investigated further to enhance the applicability of the developed empirical equations.

Author contributions S.V. wrote the main manuscript text and prepared figures. All authors reviewed the manuscript.

Funding This work was supported by Yayasan Universiti Teknologi PETRONAS, Malaysia (015LC0-304).

Declarations

Competing interests The authors have no competing interests to declare that are relevant to the content of this article.

References

1. Chen Y, Zhang H, Zhang J, Liu X, Li X, Zhou J. Failure assessment of X80 pipeline with interacting corrosion defects. Eng Fail Anal. 2015;47:67–76. https://doi.org/10.1016/j.engfailanal.2014.09.013.
2. Vijaya Kumar SD, Karuppanan S, Ovinis M. Artificial neural network-based failure pressure prediction of API 5L X80 pipeline with circumferentially aligned interacting corrosion defects subjected to combined loadings. Materials. 2022;15(6):2259.
3. Bott IDS, De Souza LFG, Teixeira JCG, Rios PR. High-strength steel development for pipelines: a Brazilian perspect. Metall Mater Trans A Phys Metall Mater Sci. 2005;36 A(2):443–54. https://doi.org/10.1007/s11661-005-0315-9.
4. Zhou R, Gu X, Bi S, Wang J. Finite element analysis of the failure of high-strength steel pipelines containing group corrosion defects. Eng Fail Anal. 2022;136:106203.
5. Zhang Y, Shuai J, Ren W, Lv Z. Investigation of the tensile strain response of the girth weld of high-strength steel pipeline. J Constr Steel Res. 2022;188(2021):107047. https://doi.org/10.1016/j.jcsr.2021.107047.
6. Ma B, Shuai J, Liu D, Xu K. Assessment on failure pressure of high strength pipeline with corrosion defects. Eng Fail Anal. 2013;32:209–19. https://doi.org/10.1016/j.engfailanal.2013.03.015.
7. Mondal BC, Dhar AS, Hafiz HI. Burst pressure assessment of pipe bend/elbow for transmission pipelines. Thin-Walled Structures. 2022;174:109148.
8. Arumugam T, Vijaya Kumar SD, Karuppanan S, Ovinis M. The influence of axial compressive stress and internal pressure on a pipeline network: a review. Appl Sci. 2023;13(6):3799.
9. Abdulhameed D, Adeeb S, Cheng R, Martens M, The Influence of the Bourdon Effect on Pipe Elbow. in *11th International Pipeline Conference*, 2016, pp. 1–10.
10. Obeyesekere NU. Pitting corrosion. Amsterdam: Elsevier Ltd; 2017.
11. Yu H, Xu X, Yu Z. Pitting-corrosion on internal wall of tee-pipe joined with main-pipe for seawater tank-washing system of a tanker. Eng Fail Anal. 2019;104(June):439–47. https://doi.org/10.1016/j.engfailanal.2019.06.013.
12. Bubenik TA, Rosenfeld MJ. Assessing the strength of corroded elbows. United States: Topical report; 1993.
13. "Pipeline Transportation Safety Investigation Report P22H0023," Gatineau, 2024. [Online]. Available: www.tsb.gc.ca.
14. Xi G, Tan F, Yan L, Huang C, Shang T. Design of an oil pipeline nondestructive examination system based on ultrasonic testing and magnetic flux leakage. Revista de la Facultad de Ingeniería. 2016;31:132–40. https://doi.org/10.21311/002.31.5.14.
15. Muthanna BGN, Bouledroua O, Meriem-Benziane M, Setvati MR, Djukic MB. Assessment of corroded API 5L X52 pipe elbow using a modified failure assessment diagram. Int J Press Vessels Pip. 2021;190:104291.
16. Shuai Y, Zhang X, Huang H, Feng C, Cheng YF. Development of an empirical model to predict the burst pressure of corroded elbows of pipelines by finite element modelling. Int J Press Vessels Pip. 2022;195:104602.
17. DNV, "Recommended Practice DNV-RP-F101." DNV, Oslo, Norway, 2017.
18. American Society of Mechanical Engineers, *Manual for Determining the Remaining Strength of Corroded Pipelines: Supplement to ASME B31 Code for Pressure Piping*. New York, USA, 2015.
19. Belachew CT, Ismail MC, Karuppanan S. Burst strength analysis of corroded pipelines by finite element method. J Appl Sci. 2011;11(10):1845–50. https://doi.org/10.3923/jas.2011.1845.1850.
20. Cronin DS, Finite element analysis of complex corrosion defects. pp. 55–61, 2002, doi: https://doi.org/10.1115/PVP2002-1288.
21. Li SJ, Zhou CY, Li J, Pan XM, He XH. Effect of bend angle on plastic limit loads of pipe bends under different load conditions. Int J Mech Sci. 2017;131–132:572–85. https://doi.org/10.1016/j.ijmecsci.2017.08.019.
22. Karamanos SA. Mechanical behavior of steel pipe bends: an overview. J Press Vessel Technol Trans ASME. 2016;138(4):041203. https://doi.org/10.1115/1.4031940.
23. KhalajKhalajestani M, Bahaari MR. Investigation of pressurized elbows containing interacting corrosion defects. Int J Press Vessel Piping. 2014;123:77–85. https://doi.org/10.1016/j.ijpvp.2014.08.002.
24. KhalajKhalajestani M, Bahaari MR, Salehi A, Shahbazi S. Predicting the limit pressure capacity of pipe elbows containing single defects. Appl Ocean Res. 2015;53:15–22. https://doi.org/10.1016/j.apor.2015.07.002.
25. Arumugam T, Karuppanan S, Ovinis M. Finite element analyses of corroded pipeline with single defect subjected to internal pressure and axial compressive stress. Marine Struct. 2020;72:102746. https://doi.org/10.1016/j.marstruc.2020.102746.
26. Bhardwaj U, Teixeira AP, Soares CG. Burst strength assessment of X100 to X120 ultra-high strength corroded pipes. Ocean Eng. 2021;241:110004. https://doi.org/10.1016/j.oceaneng.2021.110004.
27. Rosado DB, De Waele W, Vanderschueren D, Hertelé S. Latest developments in mechanical properties and metallurgical features of high strength line pipe steels. Int J Sustain Construct Des. 2013. https://doi.org/10.21825/scad.v4i1.742.
28. Benjamin AC, Freire JLF, Vieira RD, Diniz JLC, de Andrade EQ, Burst tests on pipeline containing interacting corrosion defects. in 24th International Conference on Offshore Mechanics and Arctic Engineering (OMAE 2005), 2005, no. Omae 2005, pp. 1–15.
29. Vijaya Kumar SD, Lo M, Karuppanan S, Ovinis M. Empirical failure pressure prediction equations for pipelines with longitudinal interacting corrosion defects based on artificial neural network. J Mar Sci Eng. 2022. https://doi.org/10.3390/jmse10060764.